



# Experimental studies on the gamma photons-shielding competence of $\text{TeO}_2$ - $\text{PbO}$ - $\text{BaO}$ - $\text{Na}_2\text{O}$ - $\text{B}_2\text{O}_3$ glasses

M. I. Sayyed<sup>1</sup> · Farah Laariedh<sup>1,2</sup> · Ashok Kumar<sup>3,4</sup> · M. S. Al-Buriah<sup>5</sup>

Received: 2 November 2019 / Accepted: 25 November 2019 / Published online: 5 December 2019  
© Springer-Verlag GmbH Germany, part of Springer Nature 2019

## Abstract

In this work, glass composed of  $(40 + x)$   $\text{PbO}$ -5  $\text{TeO}_2$ -15  $\text{BaO}$ -(20 -  $x$ )  $\text{Na}_2\text{O}$ -20  $\text{B}_2\text{O}_3$  ( $x=0, 5, 10, 15,$  and  $20$  mol%) was prepared via melt-quenching and the gamma-shielding competency was studied. The results showed that the density and molecular weight increased from 5.006 to 7.121 ( $\text{gcm}^{-3}$ ) and 146.579 to 178.823 (g) as  $\text{Na}_2\text{O}$  was replaced by  $\text{PbO}$ . The direct and indirect bandgap energies decreased from 3.512 to 3.357 and 2.791 to 2.525 eV as the lead concentration increased from  $\text{Pb40Na20}$ - $\text{Pb60Na0}$ . We employed the Geant4 simulation code for narrow-beam geometry with a mono-energetic photon beam imposed on a glass specimen. The mass attenuation coefficient ( $\mu/\rho$ ) for the fabricated glass was determined using the Geant4 simulation code. The difference between the theoretical values (XCOM) and simulated values (Geant4) was less than 7%, confirming the accuracy of the present results. The  $\mu/\rho$  values increased quickly with the increasing  $\text{PbO}$  content at low photon energies, while increasing the energy reduced the increase of the  $\mu/\rho$  values. The linear attenuation coefficient (LAC) was also evaluated and the results showed that increasing the density increased the attenuation behavior. The  $\text{Pb60Na0}$  sample with the highest density (7.121  $\text{g/cm}^3$ ) had the largest LAC values at all energies (in the range of 0.29–1.69  $\text{cm}^{-1}$ ). The effective atomic number values of the fabricated samples were in the range of 33–70.  $\text{Pb60Na0}$  glass with the lowest half-value layer is a promising candidate for radiation-shielding applications among  $\text{Pb40Na20}$ - $\text{Pb60Na0}$  glass.

## 1 Introduction

For over a decade, the importance of radiation-shielding materials has increased. Certain measures have been established to diminish the probability of radiation hazards to the human biological system. Most nuclear and radiation technologies cause many dangerous diseases in those vulnerable to radiation [1]. Many new materials have been introduced for radiation-protection applications, from lead and concrete. Their main purpose is to absorb harmful radiation to minimize human exposure [2, 3].

The demand for transparent shielding materials in the radiation-shielding field is increasing. The mechanical and structural properties of glass mainly depend on its composition. The radiation-shielding properties are related to the density of heavy materials such as bismuth and barium. Radiation-shielding glass should be prepared at low temperatures and should have a high density to improve their radiation-shielding properties. Moreover, the primary mixture should be combined with heavy elements that give modified glass a high density [4–6].

Heavy metal oxide (HMO) glass, that is, lead, tellurite, bismuth, and antimony, have many extraordinary characteristics such as high electrical conductivity, high solubility of rare earth ions, suitable infrared transmissivity, high optical bandwidth, and low glass transition and melting temperatures. HMO-based glass improves shielding materials against ionization radiation compared to conventional glass [7–9].

The mass attenuation coefficient, linear attenuation coefficient, effective atomic number, exposure buildup factor, tenth-value layer, mean free path, electron density, and half-value layer are the main parameters that estimate the gamma-ray attenuation characteristics for any glass system

✉ M. I. Sayyed  
mabualssayed@ut.edu.sa

<sup>1</sup> Department of Physics, Faculty of Science, University of Tabuk, Tabuk, Saudi Arabia

<sup>2</sup> Tribology and Materials for Industry Laboratory, Bron, France

<sup>3</sup> University College, Benra-Dhuri, Dhuri, Punjab, India

<sup>4</sup> Department of Physics, Punjabi University, Patiala, Punjab, India

<sup>5</sup> Department of Physics, Sakarya University, Sakarya, Turkey

**Table 1** Chemical composition and density of the prepared glass samples

Sample	Mole fraction					Density (g/cm <sup>3</sup> )
	PbO	TeO <sub>2</sub>	BaO	Na <sub>2</sub> O	B <sub>2</sub> O <sub>3</sub>	
Pb40Na20	40	5	15	20	20	5.0065
Pb45Na15	45	5	15	15	20	5.3346
Pb50Na10	50	5	15	10	20	6.2138
Pb55Na5	55	5	15	5	20	6.7687
Pb60Na0	60	5	15	0	20	7.1210

**Table 2** Physical properties of the prepared glass samples

Properties	Glass samples				
	Pb40Na20	Pb45Na15	Pb50Na10	Pb55Na5	Pb60Na0
$\rho$ (gcm <sup>-3</sup> )	5.006	5.335	6.214	6.769	7.121
M (g)	146.579	154.64	162.701	170.762	178.823
$V_m$ (cm <sup>3</sup> )	29.278	28.988	26.184	25.228	25.112
$N$ ( $\times 10^{22}$ ions cm <sup>-3</sup> )	0.823	0.935	1.149	1.313	1.439
$V_m^b$	24.398	24.156	21.819	21.024	20.926
$\langle d_{B-B} \rangle \times 10^{-8}$ (m)	3.434	3.423	3.309	3.268	3.263
$r_p \times 10^{-8}$ (m)	1.996	1.913	1.785	1.708	1.657
$r_i \times 10^{-8}$ (m)	4.954	4.747	4.430	4.239	4.111
$F \times 10^{16}$ (cm <sup>-2</sup> )	0.753	0.820	0.941	1.028	1.093

[10–16]. In the present work, glass composed of (40 +  $x$ ) PbO–5 TeO<sub>2</sub>–15 BaO–(20 –  $x$ ) Na<sub>2</sub>O–20 B<sub>2</sub>O<sub>3</sub> ( $x$  = 0, 5, 10, 15, and 20 mol%) was prepared and studied for its radiation-shielding properties. The current glasses have good radiation-shielding properties since they contain heavy metal oxides such as PbO and BaO.

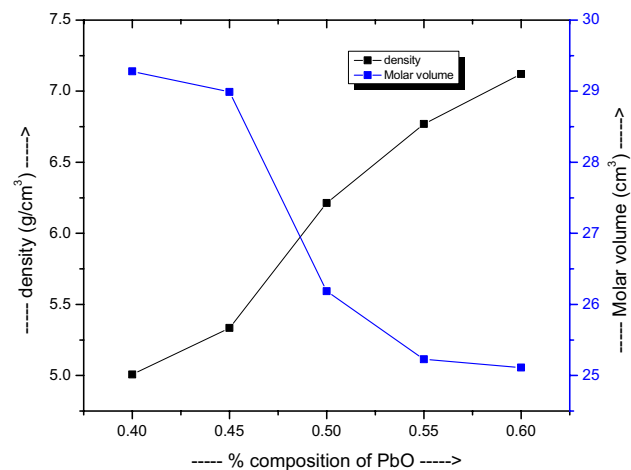
## 2 Materials and methods

Glass composed of (40 +  $x$ ) PbO–5 TeO<sub>2</sub>–15 BaO–(20 –  $x$ ) Na<sub>2</sub>O–20 B<sub>2</sub>O<sub>3</sub> ( $x$  = 0, 5, 10, 15, and 20 mol%) was prepared via melt-quenching (Table 1). High-purity oxides such as PbO, TeO<sub>2</sub>, BaCO<sub>3</sub>, NaOH, and H<sub>3</sub>BO<sub>3</sub> were used. All the chemicals were of AR grade (99.99%) and of make LOBA Company. The preparation technique was the same as described in our previous paper (Kumar et al. [17]).

## 3 Results and discussion

The formulas used for the calculation of all of the physical quantities can be obtained from our recent publication (Kaur et al. [18]).

Table 2 shows the physical properties of the Pb40Na20, Pb45Na15, Pb50Na10, Pb55Na5, and Pb60Na0 glasses. The density and molecular weight increased from 5.006 to 7.121 (gcm<sup>-3</sup>) and 146.579 to 178.823 (g) as Na<sub>2</sub>O was replaced by PbO. The increasing trend may have been due

**Fig. 1** Variations in the density and molar volume with the lead concentration

to the higher molar volume of PbO compared to sodium oxide. However, the molar volume decreased from 29.278 to 25.112 (cm<sup>3</sup>) as the lead concentration increased. This was attributed to the increase in the non-bridging oxygen and the loss of the B–O bonds that occurred [9]. The trends in the density and molar volume with the PbO content are shown in Fig. 1. The ion concentration and field strength increased from 0.823 to 1.439 ( $\times 10^{22}$  ions cm<sup>-3</sup>) and 0.753–1.093 ( $10^{16}$  cm<sup>-2</sup>). The field strength and polaron radius were opposite to one another. The polaron radius and internuclear

distance declined from 1.996 to 1.657 ( $\times 10^{-8}$  m) and 4.954 to 4.111 ( $\times 10^{-8}$  m). This decrease may have been due to the increase in the ion concentration of lead oxide from 0.40 to 0.60 mol%. The average boron separation also decreased from 3.434 to 3.263 ( $\times 10^{-8}$  m) as Pb40Na20 transitioned into Pb60Na0. This may represent the compact borate structure of the glass network [19].

Figure 2 shows the Fourier transform infrared (FTIR) spectra of the Pb40Na20, Pb45Na15, Pb50Na10, Pb55Na5, and Pb60Na0 glasses. There were many bands and small kinks at different wavelengths in these spectra. Their peak positions and assignments are shown in Table 3. Three major bands occurred at 600–800 nm, 800–1200 nm, and 1200–1500 nm. The first band near the lower wavelength side at approximately 600–800  $\text{cm}^{-1}$  occurred due to the bonding vibrations of the B–O–B groups in the different borate segments [20]. The second band in the middle region near ~ 800 to 1200  $\text{cm}^{-1}$  may have been caused by the B–O stretching vibration of the BO<sub>4</sub> in the tri-, tetra-, and pentaborate groups [21]. The higher wavenumber region ~ 1200 to 500 may have been due to the asymmetric

stretching reduction in the B–O bonds of the trigonal BO<sub>3</sub> [22]. Other small bands occurred at ~ 470  $\text{cm}^{-1}$ , ~ 510  $\text{cm}^{-1}$ , 706  $\text{cm}^{-1}$ , 950  $\text{cm}^{-1}$ , and 1360  $\text{cm}^{-1}$ . The small band at approximately ~ 470  $\text{cm}^{-1}$  may have been due to the presence of vibrating Ba<sup>2+</sup> ions in their network sites [23]. The small kink near this band at ~ 510  $\text{cm}^{-1}$  may have been due to the vibration of metal cation Na<sup>+</sup> [24]. The major band at approximately ~ 706  $\text{cm}^{-1}$  represented the bending vibrations of the B–O–B linkages in the borate network [25]. The band near ~ 950  $\text{cm}^{-1}$  was due to the vibrations of pentaborate along with tetrahedral BO<sub>4</sub><sup>−</sup> [26]. The last band near 1360  $\text{cm}^{-1}$  represented the asymmetric B–O stretching vibrations of the BO<sub>3</sub> and BO<sub>2</sub>O [25].

Tauc plots for both the direct and indirect bandgaps are shown in Figs. 3 and 4. These bandgap values were utilized to find the various optical quantities including the dielectric constant, refractive index, molar refractivity, reflection loss, optical dielectric constant, molar polarizability, and metallization. These values are shown in Table 4. Both

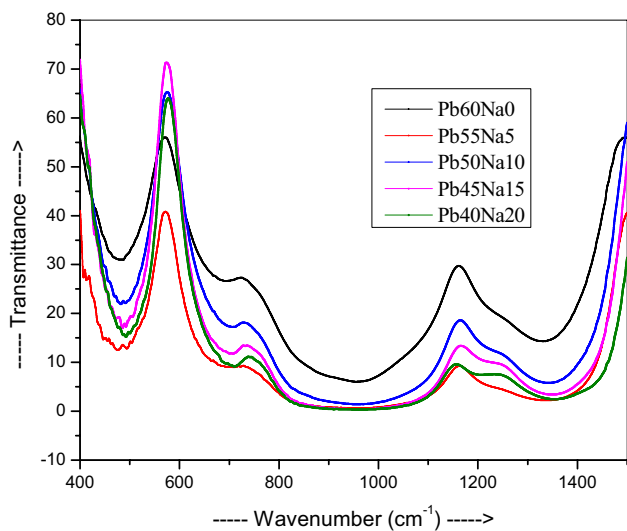


Fig. 2 FTIR spectra of the glass samples

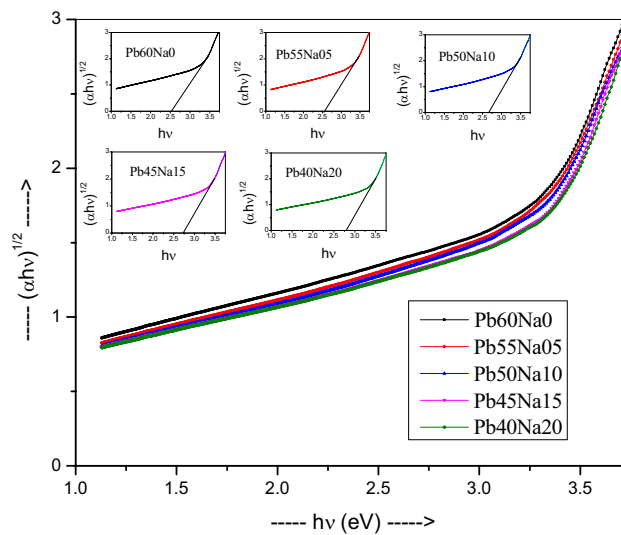
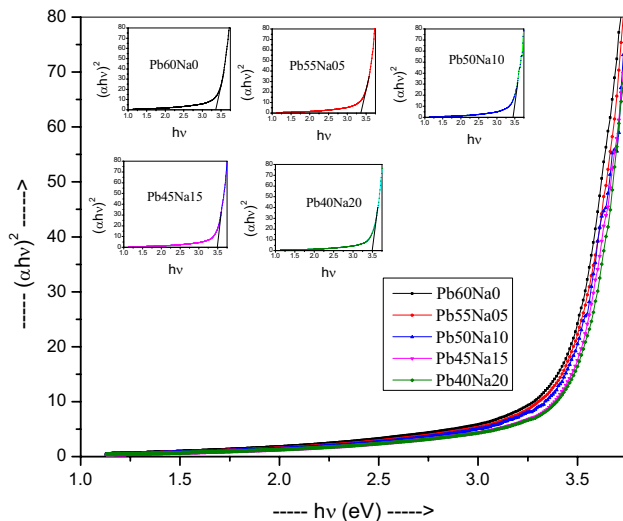


Fig. 3 Tauc plot of the indirect bandgaps

Table 3 Peak positions and FTIR assignments

Peak positions	Peak assignments
470	Vibrations of Ba <sup>2+</sup> ions in their network sites
510	Vibration of metal cation Na <sup>+</sup>
706	Bending vibrations of the B–O–B linkages in the borate network
950	Vibrations of pentaborate along with tetrahedral BO <sub>4</sub> <sup>−</sup>
1360	Asymmetric B–O stretching vibrations of BO <sub>3</sub> and BO <sub>2</sub> O
600–800	Bonding vibrations of the B–O–B groups in the various borate segments
800–1200	B–O stretching vibration of the BO <sub>4</sub> in the tri-, tetra-, and pentaborate groups
1200–1500	Asymmetric stretching reduction in the B–O bonds in the trigonal BO <sub>3</sub>



**Fig. 4** Tauc plot of the direct bandgaps

the direct and indirect bandgap energies decreased from 3.512 to 3.357 and 2.791 to 2.525 eV as the lead concentration increased in the Pb40Na20–Pb60Na0. This trend may have been due to the increase in the non-bridging oxygen, which makes glass less tight [27]. The refractive index increased from 2.456 to 2.538 as the PbO increased, while the dielectric constant increased from 6.031 to 6.443 with the increasing amount of PbO. As the PbO increased, the optical dielectric constant and reflection loss also increased, respectively, from 5.031 to 5.443 and 0.177 to 0.189. The refractive index value of glass depends on the density. As the density increases, the refractive index also increases [28]. The dielectric and optical dielectric constants depend on the ion concentration. As the ion concentration increases with the lead concentration, these values also increase [29]. However, the molar refractivity and molar polarizability of the glass in this study decreased from 18.341 to 16.189 and 7.275 to 6.421 with the increasing amount of lead oxide. The metallization values of the

present glass samples are less than unity, confirming their non-metallic nature, demonstrating that these samples can be used as non-linear optical materials [30].

Geant4 is a Monte Carlo radiation transport code used for modeling the propagation of radiation through matter [31]. This model provides the full set of electromagnetic cross sections needed to describe the interactions of photons with matter in an energy range of 1 keV–1 PeV, with uncertainties of approximately 3% [32]. We used the Geant4 simulation code for narrow-beam geometry with a mono-energetic photon beam imposed on a glass specimen. The simulation code was written using C++ language to define the gamma source, glass samples, Pb shielding, and gamma detector. One million photons were produced by a mono-energetic source to hit the glass sample target. The transmitted photons were recorded using a NaI detector. Lead was utilized to shield the NaI detector. The following energy was used in the simulation: 0.356, 0.511, 0.662, 0.826, 1.173, and 2.510 MeV. The Pb40Na20, Pb45Na15, Pb50Na10, Pb55Na5, and Pb60Na0 glasses were modeled with respect to their mass number, elemental weight fractions, and densities. The mass attenuation coefficient ( $\mu/\rho$ ) of the fabricated glass was determined using Geant4 simulation code at the aforementioned photon energies. The validation of the simulated values with theoretical predictions plays a basic role in understanding the accuracy of the present results. The Geant4 results of  $\mu/\rho$  were compared to theoretical values calculated using XCOM software [33] in Fig. 5. Table 5 shows the deviation between the theoretical results and the Geant4 values of  $\mu/\rho$  for the Pb40Na20–Pb60Na0 glasses. The theoretical and Geant4  $\mu/\rho$  results are generally in good agreement. The deviations between the Geant4 simulations and the XCOM values were evaluated using the following equation:

$$\text{Dev.} = \frac{(\mu/\rho)_{\text{XCOM}} - (\mu/\rho)_{\text{Geant4}}}{(\mu/\rho)_{\text{XCOM}}} \times 100. \quad (1)$$

**Table 4** UV parameters of the glass samples

Properties	Glass samples				
	Pb40Na20	Pb45Na15	Pb50Na10	Pb55Na5	Pb60Na0
Indirect bandgap (eV)	2.791	2.728	2.672	2.563	2.525
Direct bandgap (eV)	3.512	3.494	3.451	3.369	3.357
Refractive index ( $n$ )	2.456	2.474	2.492	2.526	2.538
Dielectric constant ( $\epsilon$ )	6.031	6.123	6.208	6.380	6.443
Optical dielectric constant	5.031	5.123	5.208	5.380	5.443
Reflection loss ( $R_L$ )	0.177	0.180	0.182	0.187	0.189
Molar refractivity ( $R_m$ ) ( $\text{cm}^3 \text{mol}^{-1}$ )	18.341	18.282	16.613	16.197	16.189
Metallization	0.374	0.369	0.366	0.358	0.355
Molar polarizability $\times 10^{-24}$ ( $\alpha_m$ ) ( $10^{-3} \text{ nm}$ )	7.275	7.251	6.589	6.424	6.421

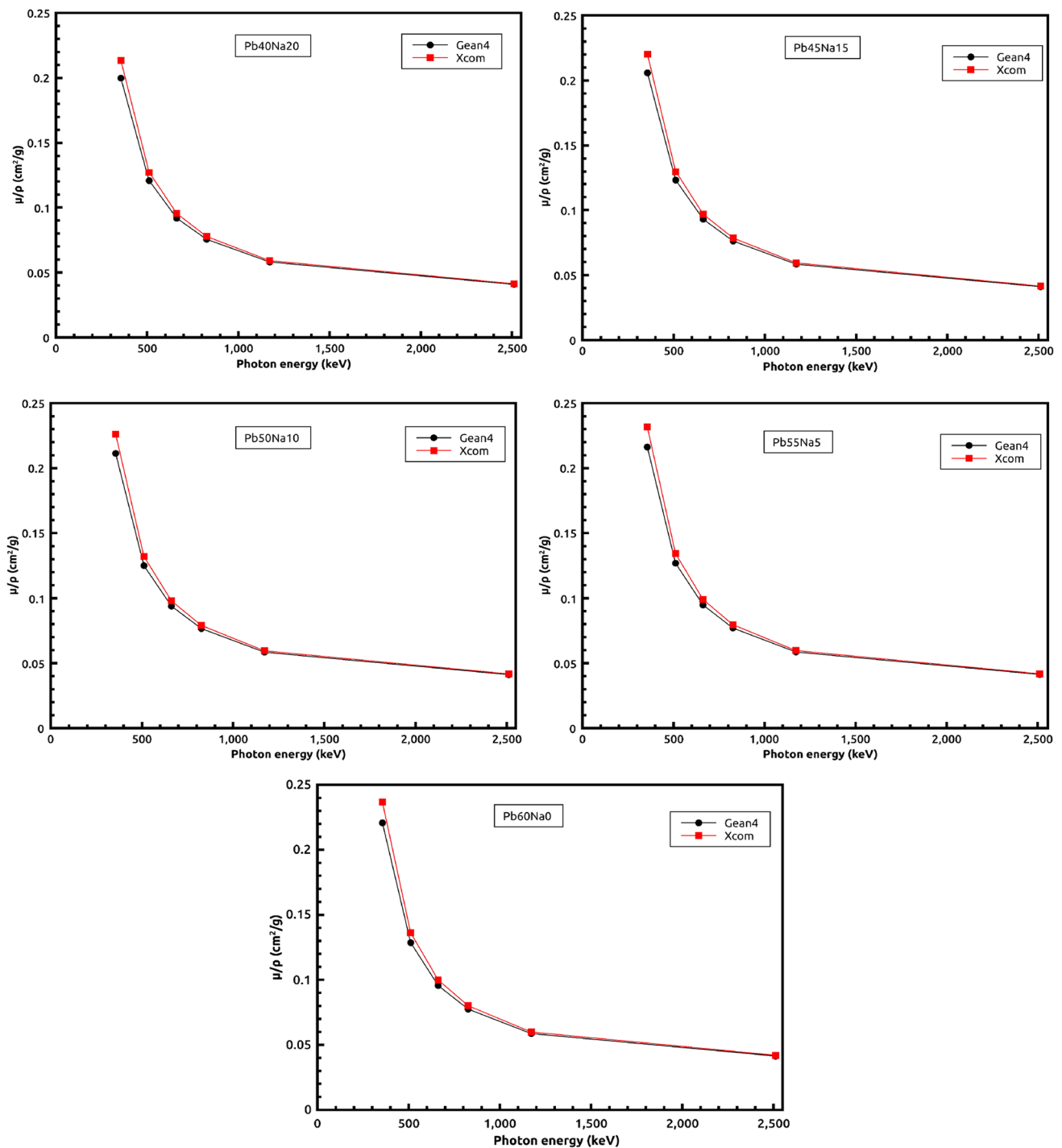


**Fig. 5** Comparison between the simulated (Geant4) and theoretical (XCOM) results of the mass attenuation coefficients of the prepared glass samples

As shown in Table 5, the deviations in the  $\mu/\rho$  values of the glass samples varied from 1.14 to 6.38% for Pb40Na20, from 1.18 to 6.49% for Pb45Na15, from 1.23 to 6.56% for Pb50Na10, from 1.28 to 6.66% for Pb55Na5, and from 1.30 to 6.74% for Pb60Na0. The high XCOM values occurred because the XCOM program settings used the mixture rule

as discussed by Singh et al. [34]. The difference between the theoretical values (XCOM) and the simulated values (Geant4) was less than 7%, confirming the accuracy of the present results.

Figure 5 shows that the  $\mu/\rho$  values of the Pb40Na20–Pb60Na0 glass exponentially decreased as the

**Table 5** The mass attenuation coefficients ( $\text{cm}^2/\text{g}$ ) of the prepared glass samples using the Geant4 code and WinXcom software

Glass code	356 keV			511 keV			662 keV			1330 keV			2510 keV		
	Geant4	WinXCom	RD	Geant4	WinXCom	RD	Geant4	WinXCom	RD	Geant4	WinXCom	RD	Geant4	WinXCom	RD
Pb40Na20	0.2135	0.1999	6.38	0.1272	0.1207	5.09	0.0954	0.0918	3.80	0.0521	0.0546	4.80	0.0415	0.0413	0.48
Pb45Na15	0.2202	0.2059	6.49	0.1298	0.1230	5.25	0.0967	0.0929	3.96	0.0524	0.0547	4.39	0.0419	0.0415	0.96
Pb50Na10	0.2262	0.21135	6.56	0.1321	0.12504	5.34	0.0979	0.093875	4.09	0.0530	0.0549	3.59	0.0420	0.0417	0.71
Pb55Na5	0.2317	0.2163	6.66	0.1343	0.1269	5.52	0.0578	0.0599	3.63	0.0532	0.0550	3.38	0.0422	0.0419	0.71
Pb60Na0	0.2367	0.2208	6.74	0.1362	0.1286	5.59	0.0580	0.0600	3.45	0.0535	0.0551	2.99	0.0427	0.0420	1.64

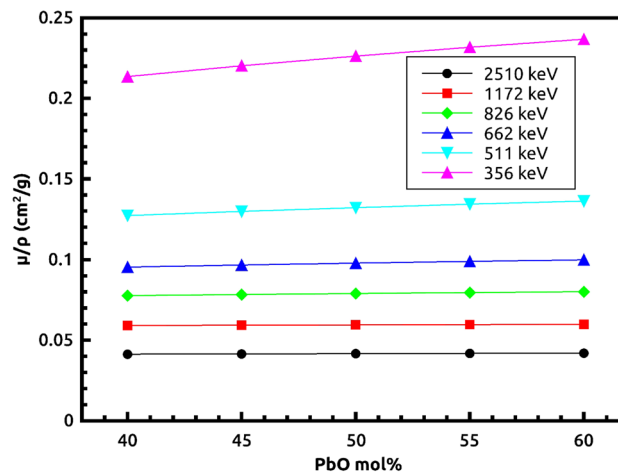


**Fig. 6** The variations in the mass attenuation coefficients of the prepared glass samples with PbO content

photon energy increased. The  $\mu/\rho$  values increased in the low-energy region ( $E = 0.356$  MeV) and decreased in the high-energy region ( $0.662$  MeV  $< E < 2.51$  MeV). The behavior of  $\mu/\rho$  can be attributed to the main photon–matter interactions [35]. The rapid decrease in the  $\mu/\rho$  values in the low-energy zone is related to the photoelectric interactions. Afterward, a slight decrease in  $\mu/\rho$  values occurred due to Compton scattering. The third main interaction for shielding gamma rays was the pair production that started at 1.022 MeV. However, this interaction dominated above 3 MeV, but this energy is out of the scope of the present work. Figure 6 shows the effect of PbO on the gamma-ray attenuation in the Pb40Na20–Pb60Na0 glasses. The  $\mu/\rho$  values increased quickly with the increasing PbO content at low photon energies, while increasing the energy reduced the increase. This occurred because the photoelectric process depends on  $Z$  (with  $Z^{4-5}$ ), whereas Compton scattering has a weak dependence on the atomic number.

Figure 7 shows a plot of the linear attenuation coefficient (LAC) vs the density of the samples. As demonstrated,  $\mu$  depends on the density of the glass; increasing the density leads to an increase in the attenuation behavior. The Pb60Na0 sample with the highest density ( $7.121$   $\text{g}/\text{cm}^3$ ) had the highest LAC values at all energies (in the range of  $0.29$ – $1.69$   $\text{cm}^{-1}$ ). This implies that the interactions between the photons and the high-density sample are relatively high and accordingly, the photons could not move throughout the sample. Pb40Na20 ( $\rho$   $5.006$   $\text{g}/\text{cm}^3$ ) had the lowest density and LAC (between  $0.207$  and  $1.609$   $\text{cm}^{-1}$ ). The photons penetrated this sample and its attenuation properties were relatively low.

The effective atomic number ( $Z_{\text{eff}}$ ) of the fabricated Pb40Na20–Pb60Na0 glasses was evaluated according to:

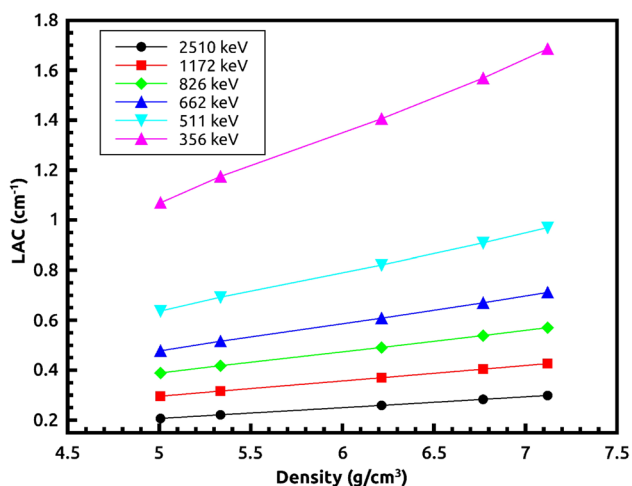


Fig. 7 The variations in the linear attenuation coefficients of the prepared glass samples with density

$$Z_{\text{eff}} = \frac{\sum_i f_i A_i \left(\frac{\mu}{\rho}\right)_i}{\sum_j f_j \frac{A_j}{Z_j} \left(\frac{\mu}{\rho}\right)_j} \tag{2}$$

This equation was used to obtain the  $Z_{\text{eff}}$  values of the Pb40Na20, Pb45Na15, Pb50Na10, Pb55Na5, and Pb60Na0 glasses. The results are plotted in Fig. 8. The  $Z_{\text{eff}}$  values of the fabricated samples were in the range of 33–70. Pb60Na0 had the most  $Z_{\text{eff}}$ , and Pb40Na20 had the least  $Z_{\text{eff}}$ . Pb60Na0 contained the highest weight fraction of Pb (0.695214%), which increased its  $Z_{\text{eff}}$ . Pb40Na20 contained the least amount of Pb (0.565431%), which explains its relatively low  $Z_{\text{eff}}$ . Good radiation-shielding glass systems should

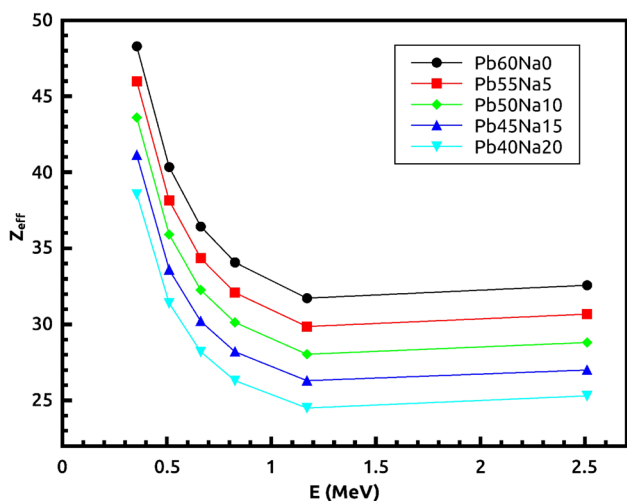


Fig. 8 The variations in the effective atomic number of the prepared glass samples with energy

have higher  $Z_{\text{eff}}$  values. This demonstrates that the gamma photons interact more with higher  $Z_{\text{eff}}$  glass, reducing the intensity of the photons so they are incapable of penetrating the glass. As shown by the  $Z_{\text{eff}}$  curves, Pb60Na0 had the best shielding features among the prepared glasses.

The half-value layer (HVL) is important for determining the shielding competence of fabricated glass against photons. The HVL values were calculated from the LAC parameter according to the following equation:

$$\text{HVL} = \frac{0.693}{\text{LAC}} \tag{3}$$

The HVL results for the Pb40Na20–Pb60Na0 glasses are plotted in Fig. 9. The HVL increased with the increasing energy. This was similar to the previous discussion of  $\mu/\rho$ . The surplus of PbO content in the prepared samples considerably improved their shielding effectiveness. The Pb60Na0 glass with the lowest HVL is a promising candidate for radiation-shielding applications.

The average distance traveled by the photons was measured via the mean free path (MFP). The MFP evaluation confirmed the present samples as a promising photon-shielding candidates. Figure 10 represents the variations in the MFP with the PbO (mol%) content in the glass samples. The addition of more PbO in the glass sample increased the number of successive collisions of the photons within the sample, reducing the MFP and improving the shielding properties. The MFP was small when the photon energy was low and increased as the photon energy increased. Consequently, in practical applications, it is better to incrementally increase the thickness of glass because photons are able to more deeply penetrate it. Figure 10 shows the economic and commercial reasons for using the prepared glass as radiation-shielding material. The MFP values changed slightly

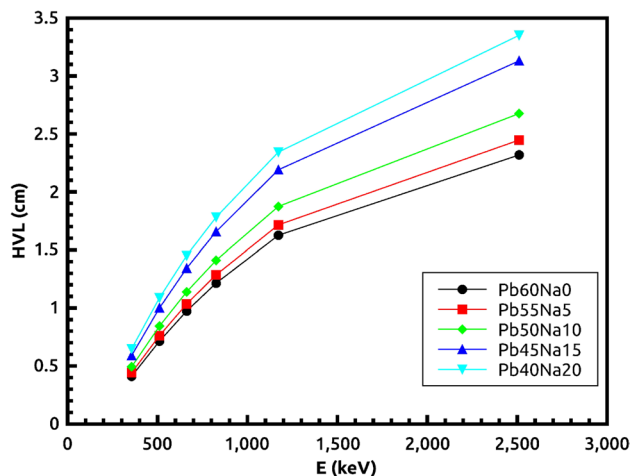
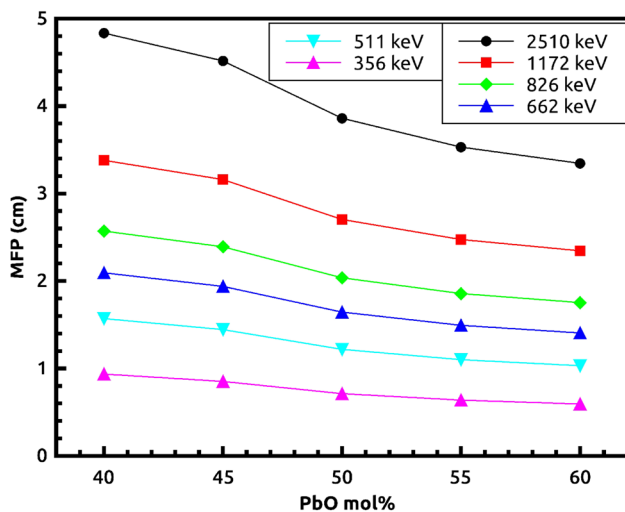


Fig. 9 The variations in the half-value layers of the prepared glass samples with energy



**Fig. 10** The variations in the mean free paths of the prepared glass samples with energy

when PbO greater than 50 mol% was added. Therefore, it is economical to use less PbO in the present glass system, especially when the radiation is higher than 662 keV (for example, in applications that frequently use radioactive sources such as Co).

## 4 Conclusions

Glass composed of  $(40+x)$  PbO–5 TeO<sub>2</sub>–15 BaO– $(20-x)$  Na<sub>2</sub>O–20 B<sub>2</sub>O<sub>3</sub> ( $x=0, 5, 10, 15,$  and  $20$  mol%) was prepared via melt-quenching. The density and molecular weight increased from 5.006 to 7.121 ( $\text{gcm}^{-3}$ ) and 146.579 to 178.823 (g) as the Na<sub>2</sub>O was replaced by PbO, while the direct and indirect bandgap energies decreased from 3.512 to 3.357 and 2.791 to 2.525 eV. The ion concentration and field strength increased from 0.823 to 1.439 ( $\times 10^{22}$  ions  $\text{cm}^{-3}$ ) and 0.753 to 1.093 ( $10^{16}$   $\text{cm}^{-2}$ ). The field strength and polaron radius were opposite to one another. The Geant4 simulation code was applied to study the radiation-shielding properties of the glass specimens. The  $\mu/\rho$  of the Pb40Na20–Pb60Na0 glasses was also determined using Geant4. The results revealed that the difference between the XCOM and simulated values (Geant4) was less than 7%. The  $\mu/\rho$  values increased rapidly as the PbO content increased at low photon energies, while increasing the energy reduced the increase. The LAC was also computed and the results demonstrated that increasing the density also increased the attenuation behavior. The Pb60Na0 sample had the highest LAC values at all energies (in the range of 0.29–1.69  $\text{cm}^{-1}$ ). The  $Z_{\text{eff}}$  values of the fabricated samples were in the range of 33–70. The surplus PbO content in the prepared samples considerably improved their shielding effectiveness.

The addition of more PbO in the glass sample increased the number of successive collisions of the photons within the sample, reducing the MFP and improving the shielding properties. The Pb60Na0 glass with the lowest HVL is a promising candidate for radiation-shielding applications.

**Acknowledgments** The authors thank the University of Tabuk for financial support under research project number S-0031-1440.

## References

1. Y.S. Rammah, M.I. Sayyed, A.S. Abohaswa, H.O. Tekin, FTIR, electronic polarizability and shielding parameters of B2O3 glasses doped with SnO2. *Appl Phys A* **124**, 650 (2018)
2. S.S. Obaid, M.I. Sayyed, D.K. Gaikwad, P.P. Pawar, Attenuation coefficients and exposure buildup factor of some rocks for gamma ray shielding applications. *Radiat. Phys. Chem.*, **148**, 86–94 (2018)
3. S.S. Obaid, M.I. Sayyed, D.K. Gaikwad, H.O. Tekin, Y. Elmahroug, P.P. Pawar, Photon attenuation coefficients of different rock samples using MCNPX, Geant4 simulation codes and experimental results: a comparison study. *Radiat. Effects Defects Solids*, **173**(11–12), 900–914 (2018)
4. D.K. Gaikwad, M.I. Sayyed, S.N. Botewad, S.S. Obaid, Z.Y. Khattari, U.P. Gawai, F. Afaneh, M.D. Shirshat, P.P. Pawar, Physical, structural, optical investigation and shielding features of tungsten bismuth tellurite based glasses. *J. Non Cryst. Solids*, **503**, 158–168 (2019)
5. M. Kurudirek, N. Chutithanapanon, R. Laopaiboon, C. Yenchai, C. Bootjomchai, Effect of Bi2O3 on gamma ray shielding and structural properties of borosilicate glasses recycled from high pressure sodium lamp glass. *J Alloy Compd* **745**, 355–364 (2018)
6. R. El-Mallawany, M.I. Sayyed, M.G. Dong, Comparative shielding properties of some tellurite glasses: part 2. *J. Non Cryst. Solids* **474**, 16–23 (2017)
7. S.A. Tijani, S.M. Kamal, Y. Al-Hadeethi, M. Arib, M.A. Hussein, S. Wageh, L.A. Dim, Radiation shielding properties of transparent erbium zinc tellurite glass system determined at medical diagnostic energies. *J. Alloys Compd.* **741**, 293–299 (2018)
8. A.M. Zoulfakar, A.M. Abdel-Ghany, T.Z. Abou-Elnasr, A.G. Mostafa, S.M. Salem, H.H. El-Bahnaswy, Effect of antimony-oxide on the shielding properties of some sodium-borosilicate glasses. *Appl Radiat Isot* **127**, 269–274 (2017)
9. A. Kumar, M.I. RamandeepKaur, M.R. Sayyed, M. Singh, Atif-Mossad Ali, Physical, structural, optical and gamma ray shielding behavior of  $(20+x)$  PbO–10 BaO–10 Na2O–10 MgO– $(50-x)$  B2O3 glasses. *Phys B* **552**, 110–118 (2019)
10. A.M. El-Khayatt, M.A. Al-Rajhi, Analysis of some lunar soil and rocks samples in terms of photon interaction and photon energy absorption. *Adv Space Res* **55**, 1816–1822 (2015)
11. D.K. Gaikwad, S.S. Obaid, M.I. Sayyed, R.R. Bhosale, V.V. Awasarmol, A. Kumar, M.D. Shirshat, P.P. Pawar, Comparative study of gamma ray shielding competence of WO3–TeO2–PbO glass system to different glasses and concretes. *Mater. Chem. Phys.* **213**, 508–517 (2018)
12. M.I. Sayyed, H.C. Manjunatha, D.K. Gaikwad, S.S. Obaid, M.H.M. Zaid, K.A. Matori, Energy-absorption buildup factors and specific absorbed fractions of energy for bioactive glasses. *Digest J. Nanomater. Biostructures* **13**, 701–712 (2018)
13. M.I. Sayyed, Bismuth modified shielding properties of zinc borotellurite glasses. *J. Alloys Compd* **688**, 111–117 (2016)



14. B. Aktas, S. Yalcin, K. Dogru, Z. Uzunoglu, D. Yilmaz, Structural and radiation shielding properties of chromium oxide doped borosilicate glass. *Radiat Phys Chem* **156**, 144–149 (2019)
15. M. Kurudirek, Heavy metal borate glasses: potential use for radiation shielding. *J Alloy Compd* **727**, 1227–1236 (2017)
16. M. Wilson, Optimization of the radiation shielding capabilities of bismuth-borate glasses using the genetic algorithm. *Mater Chem Phys* **224**, 238–245 (2019)
17. A. Kumar, D.K. Gaikwad, S.S. Obaid, H.O. Tekin, O. Agar, M.I. Sayyed, Experimental studies and Monte Carlo simulations on gamma ray shielding competence of (30 + x) PbO–10WO<sub>3</sub>–10Na<sub>2</sub>O–10MgO–(40 – x)B<sub>2</sub>O<sub>3</sub> glasses. *Prog. Nuclear Energy* (2019). <https://doi.org/10.1016/j.pnucene.2019.103047>
18. R. Kaur, V. Bhatia, D. Kumar, S.M.D. Rao, S.P. Singh, A. Kumar, Physical, structural, optical and thermoluminescence behavior of Dy<sub>2</sub>O<sub>3</sub> doped sodium magnesium borosilicate glasses. *Results Phys.* **12**, 827–839 (2019)
19. M.I. Sayyed, A. Aşkın, A.M. Ali, A. Kumar, M. Rashad, A.M. Alshehri, M. Singh, Extensive study of newly developed highly dense transparent PbO–WO<sub>3</sub>–BaO–Na<sub>2</sub>O–B<sub>2</sub>O<sub>3</sub> glasses for radiation shielding applications. *J. Non Cryst. Solids* **521**, 119521 (2019)
20. S. Khan, G. Kaur, K. Singh, Effect of ZrO<sub>2</sub> on dielectric, optical and structural properties of yttrium calcium borosilicate glasses. *Ceram. Int.* **43**, 722–727 (2017)
21. R. Kaur, S. Singh, O.P. Pandey, Influence of CdO and gamma irradiation on the infrared absorption spectra of borosilicate glass. *J. Mol. Struct.* **1049**, 409–413 (2013)
22. A.A. El-Maaref, K.H.S. Shaaban, M. Abdelawwad, Y.B. Saddeek, Optical characterizations and Judd-Ofelt analysis of Dy<sup>3+</sup> doped borosilicate glasses. *Opt. Mater.* **72**, 169–176 (2017)
23. H. Doweidar, G. El-Damrawi, E.F. El Agammy, FTIR investigation and mixed cation effect of Li<sub>2</sub>O–BaO–B<sub>2</sub>O<sub>3</sub> glasses. *Mater Chem Phys* **207**, 259–270 (2018)
24. E. Salama, H.A. Soliman, G.M. Youssef, S. Hamad, Thermoluminescence properties of borosilicate glass doped with ZnO. *J Lumin* **186**, 164–169 (2017)
25. V.V. Priya, G. Upender, M. Prasad, FTIR and ESR studies of VO<sup>2+</sup> and Mn<sup>2+</sup> doped glasses of system 59 B<sub>2</sub>O<sub>3</sub>–10 As<sub>2</sub>O<sub>3</sub>–(30 – x) PbO–x BaO. *Glass Phys. Chem.* **40**, 144–150 (2014)
26. P. Goyal, Y.K. Sharma, S. Pal, U.C. Bind, S.-C. Huang, S.-L. Chung, The effect of SiO<sub>2</sub> content on structural, physical and spectroscopic properties of Er<sup>3+</sup> doped B<sub>2</sub>O<sub>3</sub>–SiO<sub>2</sub>–Na<sub>2</sub>O–PbO–ZnO glass systems. *J. Non Cryst. Solids* **463**, 118–127 (2017)
27. F. Laariedh, M.I. Sayyed, A. Kumar, H.O. Tekin, R. Kaur, T.-B. Badeche, Studies on the structural, optical and radiation shielding properties of (50 – x)PbO–10WO<sub>3</sub>–10Na<sub>2</sub>O–10MgO–(20 + x) B<sub>2</sub>O<sub>3</sub> glasses. *J. Non Cryst. Solids* **512**, 159–166 (2019)
28. M.D. Hassib, K.M. Kaky, A. Kumar, E. Şakar, M.I. Sayyed, S.O. Baki, M.A. Mahdi, Boro-silicate glasses co-doped Er<sup>3+</sup>/Yb<sup>3+</sup> for optical amplifier and gamma radiation shielding applications. *Phys. B Condens. Matter* **567**, 37–44 (2019)
29. A.M. Ali, M.I. Sayyed, A. Kumar, M. Rashad, A.M. Alshehri, R. Kaur, Optically transparent newly developed glass materials for gamma ray shielding applications. *J. Non Cryst. Solids* **521**, 119490 (2019)
30. M.I. Sayyed, A. Kumar, H.O. Tekin, R. Kaur, M. Singh, O. Agar, M.U. Khandaker, Evaluation of gamma ray and neutron shielding features of heavy metals doped Bi<sub>2</sub>O<sub>3</sub>–BaO–Na<sub>2</sub>O–MgO–B<sub>2</sub>O<sub>3</sub> glass systems. *Prog. Nuclear Energy* **118**, 103118 (2020)
31. S. Agostinelli et al., GEANT4—a simulation toolkit. *Nuclear instruments and methods in physics research section A: accelerators, spectrometers, detectors and associated equipment. IEEE Trans. Nuclear Sci.* **506**(3), 250–303 (2003)
32. K. Amako et al., Comparison of Geant4 electromagnetic physics models against the NIST reference data. *IEEE Trans. Nuclear Sci.* **52**(4), 910–918 (2005)
33. M.J. Berger, J.H. Hubbell, S.M. Seltzer, J. Chang, J.S. Coursey, R. Sukumar, et al., XCOM: Photon Cross Section Database (version 1.5) [Online]. <https://www.nist.gov/publications/xcomphoton-cross-section-database-version-12>
34. V.P. Singh, S.P. Shirmardi, M.E. Medhat, N.M. Badiger, Determination of mass attenuation coefficient for some polymers using Monte Carlo simulation. *Vacuum* **119**, 284–288 (2015)
35. O. Agar, M.I. Sayyed, F. Akman, H.O. Tekin, M.R. Kaçal, An extensive investigation on gamma ray shielding features of Pd/Ag-based alloys. *Nuclear Eng. Technol.* **51**, 853–859 (2019)

**Publisher's Note** Springer Nature remains neutral with regard to jurisdictional claims in published maps and institutional affiliations.